

MISR photogrammetric data reduction for geophysical retrievals

Veljko M. Jovanovic, Michael M. Smyth, Jia Zong, Robert Ando and Graham W. Bothwell

Mail Stop 169-315
Jet Propulsion Laboratory, California Institute of Technology
4800" Oak Grove 1 Drive
Pasadena, CA 91109, USA

MISR photogrammetric data reduction for geophysical retrievals

Veljko M. Jovanovic, Michael M. Smyth, Jia Zong, Robert Ando and Graham W. Bothwell

Abstract--The theoretical concept, based on modern photogrammetric methods, underlying the design of the MISR science data processing system responsible for the autonomous and continuous georectification of multi-angle imagery is the subject of this paper. The algorithm partitions effort between the MISR Science Computing Facility and the EOS Distributed Active Archive Center in a way that minimizes the amount of processing required at the latter location in order to rectify and map project remotely sensed data on-line, as it comes from the instrument. The algorithm deals with the following issues: a) removal of the errors introduced by inaccurate navigation and attitude data, b) removal of the distortions introduced by surface topography, c) attainment of a balance between limited hardware resources, huge data volume and processing requirements, autonomous and non-stop aspects of the production system.

I. INTRODUCTION

The Multi-angle imaging Spectro-Radiometer (MISR) is part of the Earth Observing System (EOS) AM-1 payload to be launched in 1998 [3]. The purpose of MISR is to study the ecology and climate of the Earth through the acquisition of systematic, global multi-angle imagery in reflected sunlight. In order to derive geophysical parameters such as aerosol optical depth, bidirectional reflectance factor, and hemispheric reflectance, measured incident radiances from the multi-camera instrument must be coregistered. Furthermore, the coregistered image data and any subsequently derived product (e.g. cloud top heights) must be geolocated in order to meet experiment objectives such as: a) producing a data set of value to long-term monitoring programs and allowing intercomparisons of data on time scales exceeding that of an individual satellite, and b) providing Earth Observing System synergism by allowing data exchange between EOS-platform instruments.

The requirements for coregistration and geolocation (i.e., orthorectification), as well as stereo retrieval of a surface height from multi-temporal, multi-angle image data has been recognized since the early days of remote sensing. In order to do this, geometric distortions must be removed. The distortions are related to a number of factors, including: a) rotation of the earth during image acquisition, b) the finite scan rate of some sensors, c) the wide field of view of some sensors, d) the curvature of the earth, e) sensor non-idealities, f) variations in platform altitude, attitude and velocities, and g) panoramic and topographic effects related to the imaging geometry. A number of methods has been used to remove these distortions, from the simplest image warping techniques known as "rubber sheeting" to the rigorous implementation of imaging geometry including a camera geometric model. In most applications tile geometric data correction is not part of standard processing. Usually, standard digital data products have been only radiometrically and spectrally corrected before being distributed to investigators, who may then need to build an off-line geometric

processing system [2].

in the case of the spaceborne MISR instrument with its unique configuration of nine fixed pushbroom cameras, continuous and autonomous coregistration and geolocation of the image data is required prior to application of scientific retrieval algorithms. To address this problem, the MISR ground data processing system includes geometric processing. The algorithms used are based on modern digital photogrammetry methods. This paper describes an integrated process using techniques including: a) area-based / feature-based image matching, b) image point intersection, c) space resection and d) simultaneous bundle adjustment, and e) image-to-image registration in support of MISR systematic data processing. Section II describes the geometry of MISR instrument. Section III describes the data products produced by standard data processing using photogrammetry-based algorithms. The remaining sections describe the theoretical concepts underlying the algorithms.

11. GEOMETRY OF THE MISR IMAGING EVENT

The baseline orbit for the EOS AM-1 spacecraft has been selected by the EOS project to be sun-synchronous, with an inclination of 98.186° . The orbit period of 98.88 minutes and orbit precession rate of $0.986^\circ/\text{day}$ imply a ground repeat cycle of the spacecraft nadir point of 16 days. The orbit altitude varies from about 704 km to a maximum of 730 km. The orbit will have an equatorial local crossing time of 10:30 a.m. Figure 1 shows MISR nominal ground coverage during a one day period.

The MISR instrument consists of nine pushbroom cameras. The cameras are arranged with one camera pointing toward the nadir (designated An), one bank of four cameras pointing in the forward direction (designated Af, Bf, Cf, and Df in order of increasing off-nadir angle), and one bank of four cameras pointing in the aftward direction (using the same convention but designated Aa, Ba, Ca, and Da). Images are acquired with nominal view angles, relative to the surface reference ellipsoid, of 0° , 26.10° , 45.6° , 60.0° , and 70.5° for An, Af/Aa, Bf/Ba, Cf/Ca, and Df/Da, respectively. The instantaneous displacement in the along-track direction between the Df and Da views is about 2800 km (see Figure 2), and it takes about 7 minutes for a ground target to be observed by all nine cameras.

Each camera uses four charge-coupled device line arrays parallel in a single focal plane. The line array contains 1504 photoactive pixels, each $21 \mu\text{m} \times 18 \mu\text{m}$. Each line array is filtered to provide one of four MISR spectral bands. The spectral band shapes are approximately Gaussian, and centered at 446, 558, 672, and 866 nm. Because of the physical displacement of the four line arrays within the focal plane of each camera, there is an along track displacement in the Earth views at the four spectral bands. This must be removed during ground data processing.

The cross-track instantaneous field of view and sample spacing of each pixel is 275 m for all

of the of f-nadir cameras, and 250 m for the nadir camera. Along-track instantaneous field of views depend on view' angle, ranging from 250 m in the nadir to 707 m at the most oblique angle. Sample spacing in the along-track direction is 275 m in all cameras.

in order to find the geolocation corresponding to a pixel's field of view, the pixel pointing direction is expressed in the geocentric coordinates system, as follows:

$$\hat{\rho} = T_1 T_2 \hat{r} \quad (1)$$

where \hat{r} is the pixel pointing direction relative to the spacecraft coordinate system. The vector \hat{r} is defined by the observable image coordinates and the set of constants which represent the instrument interior orientation parameters. T_2 represents the transformation between the instrument and spacecraft coordinate axes. T_1 , defined by the ephemeris and attitude data at the time of imaging, represents the transformation between the spacecraft and Geocentric coordinate system. Equation (1) is an often used photogrammetric model [12] suitable for various image-ground point determinations required for satellite based imagery.

II. 1'1 lo'P(O;{AhNIICr'it}" I{ ASIC) I) ATA PRODUCTS

in order to satisfy coregistration and geolocation requirements the multi-angle multispectral data are processed to a common map projection. We have selected Space Oblique Mercator [13] as the reference map projection grid, because it is designed for continuous mapping of satellite imagery. The ground resolution of the map grid is 275 m. We define this segment of ground processing as "georectification", and the derived product as the Georectified Radiance Product.

There are two basic parameters in the Georectified Radiance Product depending on the definition of the reflecting surface: a) ellipsoid-projected radiance, and b) terrain-projected radiance. The ellipsoid-projected radiance is referenced to the surface of the WGS84 ellipsoid (no terrain elevation included) and the terrain-projected radiance is referenced to the same datum including a digital elevation model over land and inland water.

An ideal instrument would collect each angular view for the terrain-projected and ellipsoid-projected radiance parameters for a ground point at the same instant, giving the radiance for each band and angle for that ground point (the so-called "virtual" MISR instrument). Of course, the real MISR instrument cannot do this. It is the job of geometric processing to produce data as if it were collected by the "virtual" MISR (compare Figure 2 to Figure 3 and Figure 4).

The spatial horizontal accuracy goal associated with these products and required by the science algorithms, is an uncertainty better than ± 275 m at a confidence level of 95%. Obviously this kind of accuracy requires knowledge of a digital elevation model and removal of the displacement due to relief. In addition, the accuracy specifications for the supplied spacecraft navigation and at-

altitude data suggest the possibility of horizontal errors of about 2 km in the most oblique cameras. Section IV discusses the algorithms which account for the displacement due to the topography and errors in the spacecraft navigation data prior to the resampling of the acquired MISR imagery to the map grid.

In addition to the Georectified Radiance Product, a photogrammetry-based algorithm is used to derive cloud height parameters for the Level 2 Top of Atmosphere/Cloud product. MISR multiple views obtained from satellite altitude over a wide angular range provide the ability to separate the effects of cloud wind displacement from cloud height. In particular, a reference projection level known as the Reflecting Level Reference Altitude will be established using a stereophotogrammetric algorithm. This is defined to be the level found by matching features [11] with the greatest contrast in the near-nadir viewing directions. Physically, this corresponds to the main reflecting layer, which will typically be either the tops of bright clouds or, under atmospheric conditions corresponding to clear skies or thin cloud, the surface of the Earth.

IV. OVERVIEW OF PHOTOGRAMMETRY BASED PROCESSING

In response to the specific spatial accuracy requirements, together with the need for autonomous and continuous production capabilities, we adopted a processing strategy which partitions effort between the MISR Science Computing Facility and the EOS Distributed Active Archive Center in a way that minimizes the amount of processing required at the latter location. Activities at the Science Computing Facility lower the computational need at the Distributed Active Archive Center by precalculating certain datasets early in the mission and staging them for on-going use, in a manner that avoids much calculation during routine ground processing. These datasets include the camera geometric model, reference mbit imagery, and projection parameters (described in Section V.) Their preparation need occur only a few times during the mission, but is highly computationally intensive, involving techniques such as ray casting, and the matching of imagery from different camera angles. Consequently, routine processing of MISR data at the Distributed Active Archive Center, the characteristics of which are dominated by the very high data volume, is optimized to require only the less computationally intensive work, such as matching of imagery from the same camera angle (not different camera angles) with no need for ray casting nor a high resolution digital elevation model. Figure 5 illustrates partitioning of photogrammetric operations between the Science Computing Facility and the Distributed Active Archive Center.

From the entire MISR production system, three segments can be singled out as photogrammetric in nature. These are: 1) in-flight geometric calibration, 2) georectification and 3) cloud height retrieval.

In-flight geometric calibration is designed in response to specific requirements for standard processing: a) a balance between limited hardware resources, huge data volume and processing anti b) autonomous and on-going production throughout the mission. The in-flight geometric calibra-

tion operations are not part of standard processing. Instead, they will occur at the Science Computing Facility with the objective of producing a Geometric Calibration Dataset during the first 6 to 8 months of the mission. This dataset is used as an input to georectification processing in order to reduce processing load and provide the best possible input to automatic image registration. To produce a good quality Geometric Calibration Dataset requires precise determination of the camera's interior geometry as well as determination of the instrument's exterior orientation, taking into account errors in the supplied navigation and attitude. For (but purpose, photogrammetric techniques will be used, such as: 1) space resection 2) simultaneous bundle adjustment and 3) combined feature/area based image matching.

Given the Geometric Calibration Dataset as an input, the georectification during standard processing is significantly simplified. In particular, the most challenging part of the georectification is the image-to-image registration between new MISR imagery and reference imagery prepared as part of in-flight geometric calibration (see Section V. B). It is possible to have this process robust and fully autonomous due to the fact that registration will occur between images with the same viewing geometry. Essentially an image point intersection algorithm is employed, as the backward projection based on the camera model and supplied navigation, in order to obtain an initial guess for the tie points to be used during registration [12]. Precise location of the tie points, prior to resampling, is obtained through least-square area-based matching. The terrain-projected radiance produced during georectification is used as the input to Level 2 Aerosol/SLId_acc retrievals and cloud mask generation. Another part of the georectified product, ellipsoid-projected radiance, is used for Level 2 Top-of-Atmosphere/Cloud stereoscopic retrievals,

The photogrammetric approach to cloud top height retrieval is a singular problem if cloud motion is not known. In order to fully use the MISR image data to perform stereo retrieval of cloud top heights, we must be able to separate the effects of cloud motion and cloud height in the image disparities. This has been proven mathematically to be possible under certain imaging conditions. The MISR instrument satisfies these conditions if we perform stereo matching and retrieval with the right combination of asymmetric MISR cameras.

V. IN-FLIGHT GEOMETRIC CALIBRATION

In order to give insight into photogrammetric algorithms used during in-flight calibration we first describe the Geometric Calibration Dataset resulting from this calibration. This dataset consists of two major parts: 1) Camera Geometric Model and 2) Projection Parameters and Reference Orbit Imagery.

A. Camera Geometric Model

The Camera Geometric Model dataset consists of a set of parameters which are used in a mathematical expression that gives the pointing direction of an arbitrary pixel. These parameters

reflect geometries of the camera system and account for distortions (including temperature dependencies) from an ideal optical system [8]. There will be nine sets of parameters corresponding to the nine MISR cameras.

A mathematical expression relating line and sample (l, s) coordinates of a band in one of the MISR cameras to the vector \hat{r}_{scs} in spacecraft coordinate system can be written as:

$$\hat{r}_{scs} = T_{si} \cdot T_{ic} \cdot T_{cd} \cdot \begin{bmatrix} -(k + (l - INT(l + 0.5))d_x) \\ f \sum_{i=0}^5 \alpha_i (s - c_y)^i \\ f \end{bmatrix} \quad (2)$$

where:

T_{si} is the rotation matrix function of the angles between the spacecraft and instrument coordinate systems.

T_{ic} is the rotation matrix function of the angles between the instrument and camera coordinate systems.

T_{cd} is the rotation matrix function of the angles between camera and detector coordinate systems. k is the separation of the particular band from the intersection of the Z axis with focal plane (see figure 6)

c_y is the pixel number (i.e., boresight pixel) corresponding to the X axis (Y=0).

d_x is the detector pitch in X direction.

f is the effective focal length.

$\alpha_i, i = 0, 1, 2, 3, 4, 5$ are the coefficients of a fifth-order polynomial to account for the nonlinear distortions of the field angle in the cross-track direction.

Equation (2) is the explicit way of defining the pointing direction of an individual pixel relative to the appropriate coordinate system. The number and type of parameters depend on the individual sensor characteristics. In photogrammetric terminology MISR Camera Geometric Model data are called the "interim orientation parameters". Using the same terminology, the supplied navigation data defines what are called "exterior orientation parameters". Thus the Camera Geometric Model in conjunction with the supplied navigation data will provide the pointing vector of an arbitrary pixel, relative to the Earth-fixed Earth-centered coordinate system. This pointing vector is the fundamental information used during standard georectification for both the terrain-projected and ellipsoid-projected radiances.

B. Projection Parameters and Reference Orbit Imagery

The full set of Reference Orbit imagery (ROI) consists of selected cloud free MISR imagery mosaicked and stored in the 233 files corresponding to the 233 orbit paths of the TiOS-Ah41 spacecraft. Organized similarly into 233 files are the Projection Parameters (PP), which are produced off-line using rigorous photogrammetric reduction methods. The PP files provide geolocation information for acquired MISR imagery on a pixel by pixel basis. This geolocation information is referenced to a selected Space Oblique Mercator map projection grid. The process of creating ROI and PP files is similar to the regular orthorectification of time dependent sensor imagery. The major differences are: a) acquired imagery is geolocated but not resampled, and b) a global digital elevation model of sufficient resolution is available for MISR's internal use. A simultaneous bundle adjustment utilizing multi-angle imagery and ground control information (global digital elevation model and ground control point chips) is used to model errors in the navigation and attitude data for a single set of ROI, prior to geolocation.

The coupled PP and ROI files provide two major benefits to the standard georectification processing. First, expensive computation required to account for topographic displacement will be performed only once, off-line during calibration. The obtained information will be saved in a file and utilized during on-line processing throughout the mission. This is possible because of the small orbit-to-orbit variations at the same location within an orbit path, adding relatively small changes to the topographic displacements (that can be accounted for in a separate process during georectification). Second, unresampled but geolocated MISR imagery will be used as ground control information. The idea is that MISR imagery with close to the same viewing geometry will provide a high success rate during least-square area-based image matching performed by standard processing during image-to-image registration.

C. Calibration Algorithm

This algorithm consists of two parts: Part one focuses on the removal of distortions from the Camera Geometric Model measured on the ground. These distortions result from the deformations of mechanical connections between the cameras, optical bench and the spacecraft platform, caused by launch and gravity release of the camera system. Part two focuses on the production of the specific information useful for the routine removal of the navigation and attitude errors, and distortions due to the surface topography. This information is stored in the Projection Parameters and Reference Orbit imagery files which along with the Camera Geometric Model make up the Geometric Calibration Dataset that is used as the input to the Level 1B2 georectification standard processing algorithm.

1) *In-flight Camera Geometric Model Calibration.* Some of the parameters of the camera model characterized during preflight ground calibration [8] must be verified on orbit. The exact subset of parameters to be recalibrated is still to be determined. The calibration algorithm will make use of

ground control points (GCPs) and it will focus on the recalibration of each camera individually. The idea is to isolate static and systematic (e.g., temperature dependent) errors of the individual cameras from the errors reported in the navigation data. This is possible by having a large number of observations by a single camera of well-defined and well-distributed ground targets or GCPs (Figure 7). Area-based image matching is used for automatic identification of GCPs.

A mathematical expression used to describe the ray between a ground point and the image of that point, as seen by a MISR camera, is used as the model for the least-squares estimation [10] of certain camera model parameters i.e. space resection. A large number of observations and good distribution of GCPs are needed so that the effects of errors in the navigation data on the estimation of camera model parameters can be fully minimized. In that regard, it should be pointed out that a single GCP will be seen multiple times from a single camera during a 16-day period. This is important because it significantly increases the number of observations and, at the same time, provides a good distribution of ground control points across a camera field of view.

2) *Creation of Projection Parameters and Reference Orbit Imagery.* The calibrated Camera Geometric Model may not be sufficient to provide a product of the desired geolocation and registration accuracy. After applying the calibrated camera model, two types of errors remain significant: 1) errors in the navigation data, and 2) displacements due to the surface topography. The following steps will be conducted at the MISR Science Computing Facility in order to remove the effects of those errors and create the PP and ROI files.

2.a) *Forward Projection.* A pixel in the map grid might not be seen by a particular MISR view angle because it is topographically obscured by terrain surrounding the pixel (see Figure 8). To determine this, a ray casting algorithm is used, also referred to as a forward projection. A nominal set of navigation data and camera viewing geometry is used. Subpixeling (i.e., ray casting more than one ray for a single pixel) is performed to give a nominal ground pixel size of the resolution of the digital elevation model used to describe the terrain (i.e., about 100 meters). If any one of the subpixels of a map grid pixel is not seen by a MISR camera, then the whole map grid pixel is marked as obscured at that camera angle. The information about which map pixels are obscured is stored in the PP file, for use by the georectification algorithm.

2.b) *Backward Projection.* After determining which map grid pixels are obscured, the location in the MISR imagery where the center of each map grid pixel is seen is determined for each camera angle. This is done by using a modified image point intersection algorithm, described in more detail in Section VI.B. The same nominal set of navigation data and camera viewing geometry as in step 2.a is used. This information is stored in the PP files, for use by the georectification algorithm.

After performing steps 2.a and 2.b, the PP files contain the information needed to resample MISR imagery acquired with nominal navigation data and camera viewing geometry. Of course,

we do not expect to acquire image data with navigation data and camera viewing geometry identical to the nominal set. Real data will contain perturbations in the spacecraft position and attitude. The point is that the problem of resampling real MISR imagery to the map grid has been reduced to the problem of accounting for differences between the real navigation data and camera viewing geometry and the nominal set used to produce the PP. The PP then gives the remaining information about how to perform the map projection, once the differences with the nominal case are taken into account.

2.c) Adjustment. A “simultaneous bundle adjustment” (a least square data estimation technique) constrained by a relatively high resolution digital elevation model is used to improve the accuracy of the navigation data later used to produce ROI consistent with the set of PP obtained by using nominal orbit data.

The simultaneous bundle adjustment takes advantage of the following MISR characteristics: 1) at a single instant of time MISR “sees” nine different, widely separated, targets on the ground, and 2) a single location on the ground is seen at nine different instants of time. If the errors in the navigation data are modeled as time dependent, then it is possible to write a mathematical model which will utilize known MISR characteristics and improve the accuracy of the navigation data.

This model is certainly good for improving relative accuracy (during a time period) of the navigation data. In order to obtain absolute accuracy (i.e., relative to a fixed ground coordinate system) additional ground control information is needed. For that purpose, in addition to already available GCPs, a high resolution digital elevation model is included as a good constraint to the adjustment.

Due to the fact that GCPs have to be manually collected and sparsely distributed, an automatic and robust tie-point identification algorithm is designed to provide well-distributed tie-points for the simultaneous bundle adjustment. A tie-point refers to the conjugate image feature locations of the same ground point across multiple images viewed from various angles. Based on initial conjugate image locations determined using the knowledge of MISR navigation data, interest point features are detected independently on all 9 local conjugate image patches extracted from MISR imagery [4]. A feature-based matching scheme, namely consistent labeling with forward check [6], is used to match conjugate interest points as improved tie-points, compared to the original ones. An area-based matching algorithm is then used to accurately identify the final tie-point with an uncertainty of less than 0.2 pixel. The tie-point identification is a completely automated process without human intervention. A supporting method with a human operator in the loop will be used mostly for validation purposes and for some infrequent occasions where improvement of the automatic detection of tie points is needed.

2.d) Reference Orbit Imagery. In order to determine the differences between real MISR data and the nominal navigation data and camera viewing geometry used to produce the PP, a dataset

called the Reference Orbit Imagery is produced. This data provides ground control that can be image matched to newly acquired MISR image data during the georectification process (see Section VI.C). The ROI is created by mosaicking MISR image data to maximize cloud-free regions. The image data are resampled to make it appear as if they were acquired using the nominal navigation data and camera viewing geometry used in the production of PP. This resampling is done by building an image-to-image transform (see Section VI.D) between the MISR image data and an image with nominal navigation data. The transform is built using improved navigation data generated in Step 2.c.

VI. GEORECTIFICATION ALGORITHM

A. Overview

in the systematic georectification system we make use of ancillary datasets, namely a set of Projection Parameters and Reference Orbit Imagery, produced at the beginning of the mission. The major information implicitly contained in these datasets is error free navigation and attitude data, georeference, and surface topography relative to the various geometries of the nine MISR cameras. This information is routinely exploited through a hybrid image registration algorithm (see Figure 9). In particular, the autonomous and continuous georectification is reduced to a recursive image registration between ROI and new MISR imagery which consists of the following elements:

- a) Image Point Intersection: a backward projection function used to provide an initial location of the conjugate points [12].
- b) Image matching for the precise identification of the conjugate points.
- c) Transformation (mapping) function between two images.

The registration method is adaptive with regard to the character and size of misregistration, in order to minimize the processing load. The adaptive nature of the algorithm is attained by recursively dividing images into subregions until the required registration accuracy is achieved (see Figure 10). Initially, due to the push-broom nature of the MISR cameras, subregions are rectangles extending over the image in the cross-track direction. The mapping function associated with a subregion is a mollification of the affine transform which includes known geometric characteristics of the MISR imaging event. Once the mapping between the two images is established, the last processing step is the assignment of the appropriate radiance value to the grid point of the Space Oblique Mercator map. This is done using bilinear interpolation.

Additional techniques are required so that autonomous production runs are unaffected by less-than-perfect input data. Some of the more obvious examples are the presence of cloudy regions, water bodies, and deserts. These types of conditions significantly reduce the number of conjugate points available to determine the transformation function. In such cases additional techniques must be implemented. In some cases, searching for cloud-free land in the local neighborhood may be sufficient. In other cases, where a large region of data is without conjugate points, use

of information obtained through the registration of the closest subregion is applied. The idea is to correct for slowly varying parameters through the use of a Kalman filter built while processing previous subregions.

Also included in the algorithm is a blunder detection technique aimed at removing possible blunders coming from the image matching. This utilizes statistical results obtained from the least-square estimation of the transformation function.

B. Image Point intersection

A rigorous ground-to-image projection is used to compute image coordinates of the initial tic points prior to image matching. It utilizes a well-known collinearity condition modified for MISR time-dependent imagery constrained by the equation which describes the spacecraft trajectory. It is obtained utilizing the ground point coordinates x , the position of the sensor at time of imaging P , and the pointing direction of the ray imaging the ground point (see equation (1)) all referenced to the Geocentric coordinate system:

$$X = P + \lambda p \quad (3)$$

where λ is a scale factor. Using an iterative root-finding method, equation (3) can be solved for the image coordinate of the ground point. initial input to the iterative solution is obtained from the PP file in conjunction with nominal orbit parameters.

C. Image Matching

An image matching technique has been chosen in order to: a) precisely locate tic points during image-to-image registration, and b) to estimate the accuracy of the local image-to-image transformation. Our decision to use a combination of cross-correlation and least-square area based image matching method [1] is based largely on two factors. First, the high subpixel accuracy of successful matches that can be achieved [5]. Second, MISR new and reference images with their minimal perspective changes between the two views will serve as very good input to the selected method. The sizes of the “target” and “search” windows are based on the expected errors in the supplied navigation and attitude data. For completeness we give a mathematical description of the implemented area-based matching.

First, using the results from the image point intersection the points from new and reference images are matched based on a variation of the normalized cross-correlation, computed as follows:

$$C = \frac{\sigma_{new, ref} \cdot |\sigma_{new, ref}|}{\sigma_{new}^2 \cdot \sigma_{ref}^2} \quad (4)$$

where σ_{newref} is the covariance between new and reference MISR image chips and $\sigma_{new}^2, \sigma_{ref}^2$ are the variances.

The results obtained by the cross-correlation method are improved to subpixel accuracy by least-square matching. In the least-square matching the geometric and radiometric transformations between two image chips are estimated by minimizing certain functions between them. Let:

x', y' be the coordinates in the reference image.

x'', y'' be the coordinates in the new image

Then the geometric relation is modeled by the affine transformation

$$\begin{aligned} x'' &= F_x(x', y') = a_0 + a_1 \cdot x' + a_2 \cdot y' \\ y'' &= F_y(x', y') = a_3 + a_4 \cdot x' + a_5 \cdot y' \end{aligned} \quad (5)$$

Also, if

$$\begin{aligned} g' &= G'(x', y') + n'(x, y) \\ g'' &= G''(x'', y'') + n''(x'', y'') \end{aligned} \quad (6)$$

are the discrete radiance values for reference and new image respectively, where G' and G'' are image functions, while n' and n'' are associated noise values, then the radiometric relation is expressed as a 2-parameter linear function:

$$g' = F_r(g'') = k_0 + k_1 \cdot g''(F_x, F_y) \quad (7)$$

Through iterations using linearized form of (7) we solve for parameters a_i and k_i .

D. Image-to-Image Transformation

A polynomial form to be used for image-to-image transformation between new and reference imagery was derived by looking at the physical characteristics of a push-broom camera. We built a model that describes how a scan line of the reference image maps to the new image. We then assumed that the mapping for nearby scan lines should be nearly identical. Although the model was derived for a single scan line, we apply it to a larger area (nominally 256 lines of data).

The physical aspects modeled include: a) linear optics (i.e., we ignore the small nonlinearities in the camera optics), b) earth curvature, and c) effect of ground topography.

This gives the following modification of the general affine transformation:

$$s_{new} = k_{14}(l_{ref} - l_0) + k_{15}(s_{ref} - s_0) + k_{16}(s_{ref} - s_0)^2 + k_{17}h_{surface} + k_{18} \quad (8)$$

$$l_{new} = k_{19}(l_{ref} - l_0) + k_{20}(s_{ref} - s_0) + k_{21}(s_{ref} - s_0)^2 + k_{22}h_{surface} + k_{23} \quad (9)$$

Testing shows that the corrections we have derived to the affine model are important. The quadratic term at the edges of the swath can be as large as 2 pixels. However, the height term is usually small, and in the Beta version of the M ISR software it was dropped from the model.

We use this transform in the following manner:

1. Start with a region of imagery (nominally 256 lines, full swath).
2. Find well-distributed conjugate points in the reference and new imagery. This requires finding points in areas where image matching can be performed (e.g., cloud free land).
3. Use conjugate points to determine the coefficients in (8) and (9) by doing a least squares fit.
4. Find another set of conjugate points to use as check points. Compare the prediction of the location of the conjugate points in the new image obtained by (8) and (9) to the actual location. If they are within the allowed tolerances (e.g., 1/2 pixel), then we are done. Otherwise, break the region into two smaller pieces, and repeat the process for each of the smaller pieces.

E. Blunder Detection

A blunder detection function was implemented to prevent low accuracy and extra sub-gridding effort caused by the appearance of blunders from image matching. The least-square fit of image-to-image transform can be represented by a general observation equation:

$$v = Ax - y \quad (10)$$

Where the observation y is a set of random variables, $y = (Y, \sigma_0^2 P_{yy}^{-1})$. $Y = Ax$ is the true value of the observation, σ_0 is the variance per unit weight of the observation, P_{yy} is the weight matrix, x is the set of unknown parameters. A is the design matrix relating x to y . Finally, v is the residual $v = y - Y$. The best estimated least square solution to the above linear system is to minimize $\phi = v^T P v$, which easily leads to a normal equation $\tilde{x} = Q_{xx}^{-1} A^T P_{yy}^{-1} y$, where the cofactor matrix of the estimated unknown parameters is $Q_{xx} = (A^T P_{yy}^{-1} A)^{-1}$. The residual vector and its cofactor matrix are then related by the following equation as:

$$v = A\tilde{x} - y = (AQ_{xx}A^T P_{yy}^{-1} - I)y = -(Q_{yy} P_{yy})y \quad (11)$$

Equation (11) indicates how the errors of one or more of the observations (Δy) influence the residuals. This relation can be written as $v = -(Q_{vv}P_{yy})\Delta y$. It shows the cofactor matrix of the residual Q_{vv} and the observation weight matrix P_{yy} are the key to the relationship of the observation-errors or blunders Δy , to their corresponding residual. In case of equal weight, a large diagonal value of Q_{vv} means that an observation error is translated to the corresponding residual, a small diagonal value diffuses the observation error. The off-diagonal value of Q_{vv} does the opposite. The fact of a large off-diagonal value can pass an observation error to other residual than the corresponding one is caused by the high correlation among observations. This effect can be minimized by good configuration of our control point distribution.

Assume there is no gross-error in observation but only random error and random error follows a normal (Distribution). The residuals will do the same meaning their expectation is 0 with a variance of σ_v^2 . The mean error of residual v_i can be represented as $\sigma_v = \sigma_0 \sqrt{(Q_{vv})_{ii}}$. Therefore the accuracy of the residual v_i depends not only on the observation error but also on the diagonal values of Q_{vv} . Obviously, the standardized residuals $\bar{v}_i = v_i / \sigma_{v_i}$ follows a standardized normal-distribution with expectation 0 and variance 1. The effect of diagonal value of Q_{vv} is reduced in this representation. The standardized residuals are ideal for statistical testing to detect blunders. However, statistical testing only works with few blunders and the removing of blunder is one at a fitting time and therefore called data snooping. If blunders exist during one data fitting, the post estimated variance per unit weight $\hat{\sigma}_0 = \phi / r$ (r as the redundancy of the system) testifies that first, and the test to the standardized residual instead of residual can be used to point out the causing blunder.

F. Band-to-Band Transformation

The registration between the new MISR image and ROI imagery has been done using the red spectral band (Figure 9) because of its characteristics relative to the image matching requirements. The imagery from the other three bands will be registered to the already registered and geolocated red band. This registration does not include image matching. Rather, the transformation between bands is defined by the interior orientation parameters of the geometric camera model. More details on this transformation can be found in [14].

VII. CONCLUSIONS

MISR photogrammetric data reduction is a unique and successful process. It provides effectively and precisely the geo-registered information for geophysical and other scientific research usage. With the state-of-the-art photogrammetric techniques, we have been able to meet the geo-registration requirement and multi-camera co-registration requirements with our simulated test data [9]. Figures 11 and 12 represent portions of the geometric product. They clearly show spatial accuracy of a multi-layered map projection (Figure 12) created for the terrain-projected radiance. Also, in Figure 1] epipolar geometry and suitability of the ellipsoid-projected radiance for the stereo

height retrievals are demonstrated.

VIII. ACKNOWLEDGMENTS

The authors gratefully acknowledge the efforts of the MISR Principal Investigator, David J. Diner, co-investigator Jan-peter Muller and the members of the Science Data System Team: Earl G. Hansen, Brian E. Rheingans, and Scott A. Lewicki. Additional thanks are due to Carol J. Bruegge and Robert P. Korechoff for their efforts in MISR camera calibration. This research is being carried out at the Jet Propulsion Laboratory, California Institute of Technology, under contract with the National Aeronautics and Space Administration.

IX. REFERENCES

[1] Ackermann, F., "Digital Image Correlation: Performance and Potential Application in Photogrammetry", *Photogrammetric Record*, **11,64**, 1984.

[2] Allison, D., Barnsley, M. J., Lewis P., Dyble N., and Muller, J. P., "Precise Geometric Registration of ASAS Airborne Data for Lanti Surface BRDF Studies", *IGARSS Proceedings*, **3**, 1655-1657, 1994.

[3] Diner, D. J., Beckert, J. C., Reilly, T. J., Bruegge, C. J., Conel J. E., Kahn, R. A., Martonchick, J. V., Ackerman T. P., Davis, R., Gerstl, S. A. W., Gordon, H. R., Muller, J. P., Myneni, R., Sellers, P. J., Pinty, B., and Verstraete, M. M., "Multi-angle Imaging SpectroRadiometer (MISR) Instrument Description and Experiment Overview", *IEEE Trans. Geosci. Remote Sens.*,

[4] Forstner, W., "A Fast Operator for Detection and Precise Location of Distinct Points, Corners and Centers of Circular Features", *ISPRS Intercommission Workshop, InterLaken*, 1987.

[5] Forstner, W., "On the Geometric Precision of Digital Correlation", *ISPRS Int. Arch. of Photogrammetry*, vol. XXIV, Commission II 1,1 Helsinki, i 980.

[6] Haralick, R., Shapiro, L., "Computer and Robot Vision", Addison-Wesley Publishing Company, 1993.

[7] Herrick, S., "Astrodynamics", Van Nostrand Reinhold, New York, 1971.

[8] Korechoff, R. P., Jovanovic, V. M., Hochberg, E. B., Kirby, D. M., and Sepulveda, C. A., "Distortion calibration of the MISR linear detector arrays", *SPIE Proceedings Volume 2820-19*, Denver, Colorado August 1996.

[9] Lewicki, S. A., Smyth, M. H., Jovanovic, V. M., and Hansen, E. G., "A Simulation of EOS MISR Data and Geometric Processing for the Prototyping of the MISR Ground Data System", *IGARSS Proceedings*, **3**, 1543-1545, 1994.

[10] Mikhail, E. M., "Observations and I cast Square", Harper & Row, New York, 1976.

[11] Muller, J. p., Mandanayake, A., Davis, R., and Moroney, C., "A comparison of stereo matching techniques for Global Cloud-top Height retrieval from ATSR and MISR", J. Geophys. Res., in preparation, 1997.

[12] Paderes, F. C., Mikhail, E. M., and Fagerman, J. A., "Batch and On-Line Evaluation of Stereo *spot Imagery*", ASPRS Proceedings, **3**, 1989.

[13] Snyder, J. P., "Map Projection - A Working Manual", United States Geological Survey Professional Paper 1395, U. S. Government Printing Office, Washington, 1987.

[14] Zong, J., Jovanovic, V. M., anti Smyth, M. M., "MISR band-to-band registration", *SPIE Proceedings* Volume 2818-28, Denver, Colorado August 1996.

Figure 1

MISR nominal ground coverage during a one day period. '1' here ate 16 ground tracks obtained by projecting IFOV for the nadir camera.

Figure 2

MISR imaging event.

Figure .?

Terrain-projected radiance product: output from a "virtual" MISR.

Figure 4

Ellipsoid-projected radiance product: output from a "virtual" MISR.

Figure 5

Processes and datasets of the M ISR production system related to algorithms based on photogrammetric methods.

Figure 6

Detector Coordinate System of the Camera Geometric Model. The x axis is defined to be per-

pendicular to the long axis of the detector arrays. The y axis is parallel to the long axis and is positive in the westward direction during a descending pass. The z axis is the cross product of x with y forming a right-handed coordinate system. The figure shows that the focal plane is located at $z = -f$ where f is the effective focal length of the particular camera.

Figure 7

In-flight Camera Geometric Model Calibration

Figure 8

Backward/forward projection

Figure 9

Implementation of terrain-projection algorithm

Figure 10

Recursive image-to-image registration

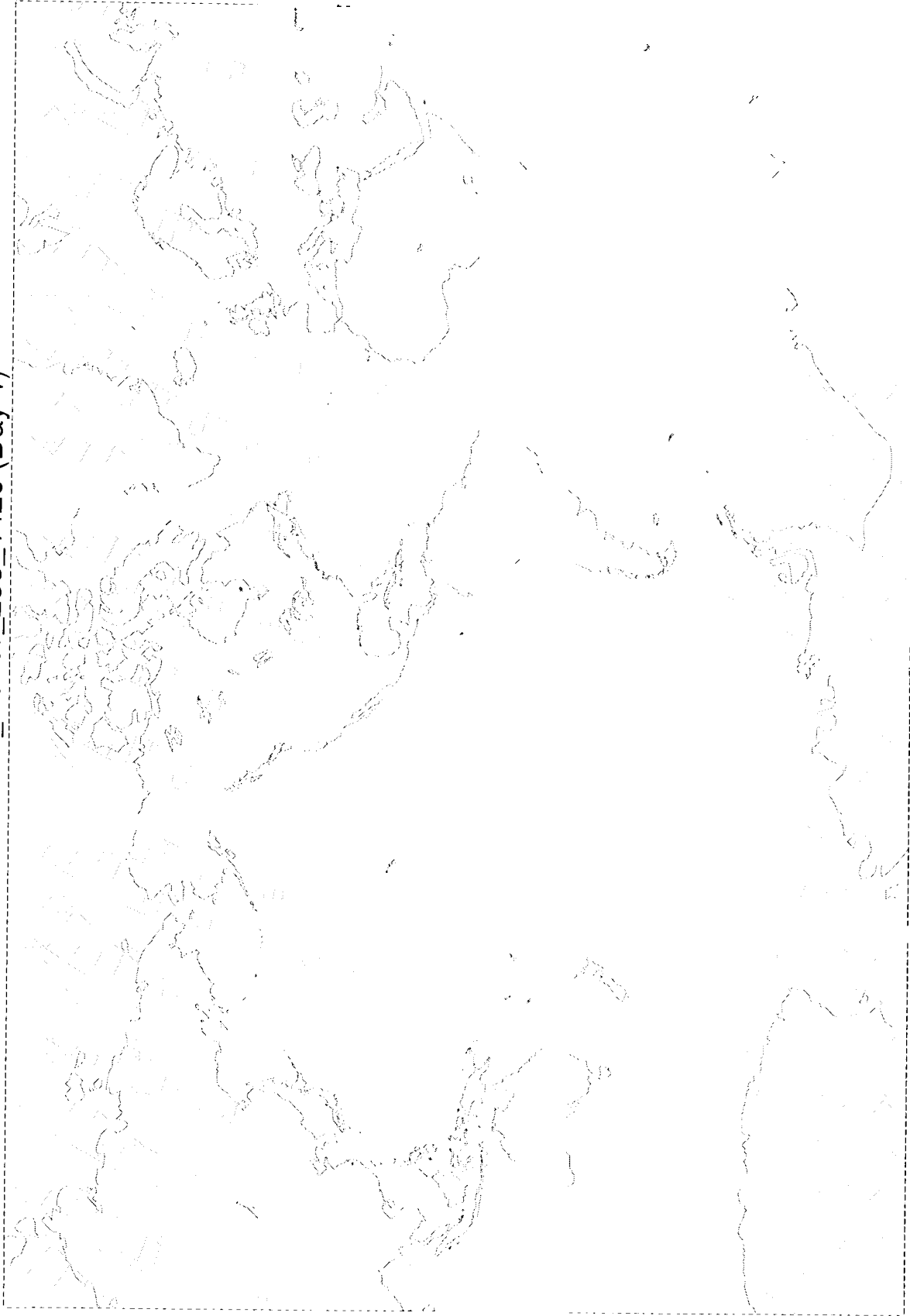
Figure 11

Ellipsoid-projected red band data for A forward (Af) and C aft (Ca) cameras are superimposed to make this color composite. The Af camera image data are color coded red and the Ca camera image data are color coded blue and green to make a pseudo color image suitable for stereo viewing with standard red and blue filter glasses. This shows the effect of the along-track parallax preserved in the ellipsoid-projected data which are used for stereo cloud height retrievals.

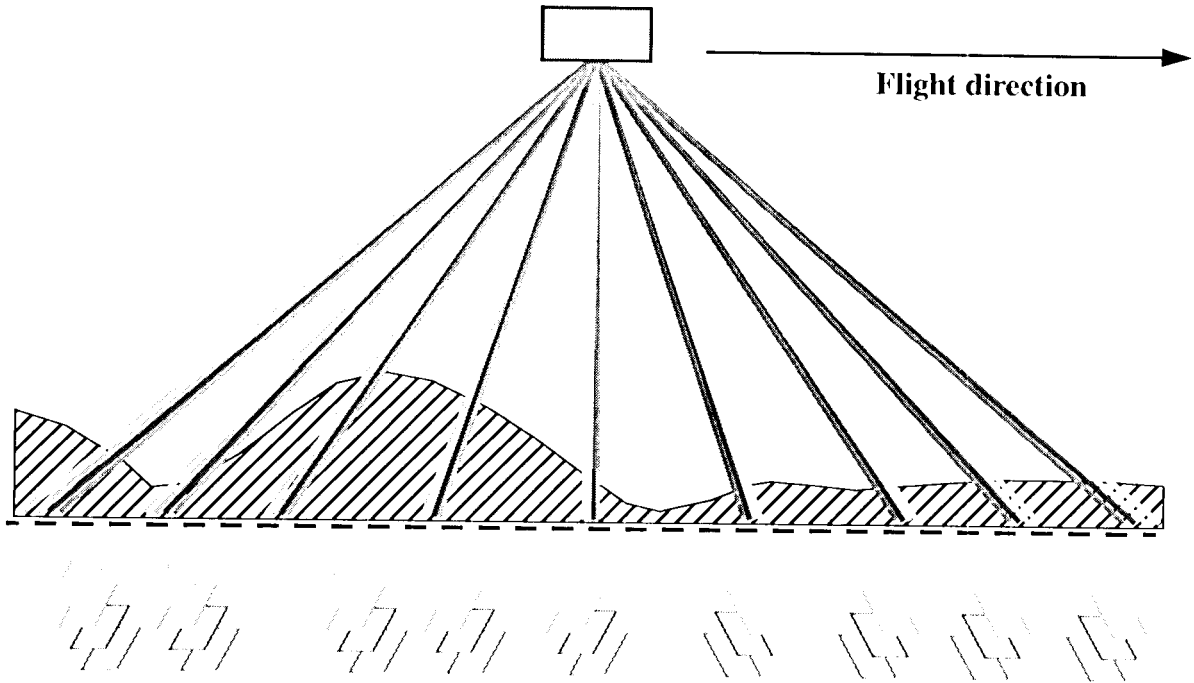
Figure 12

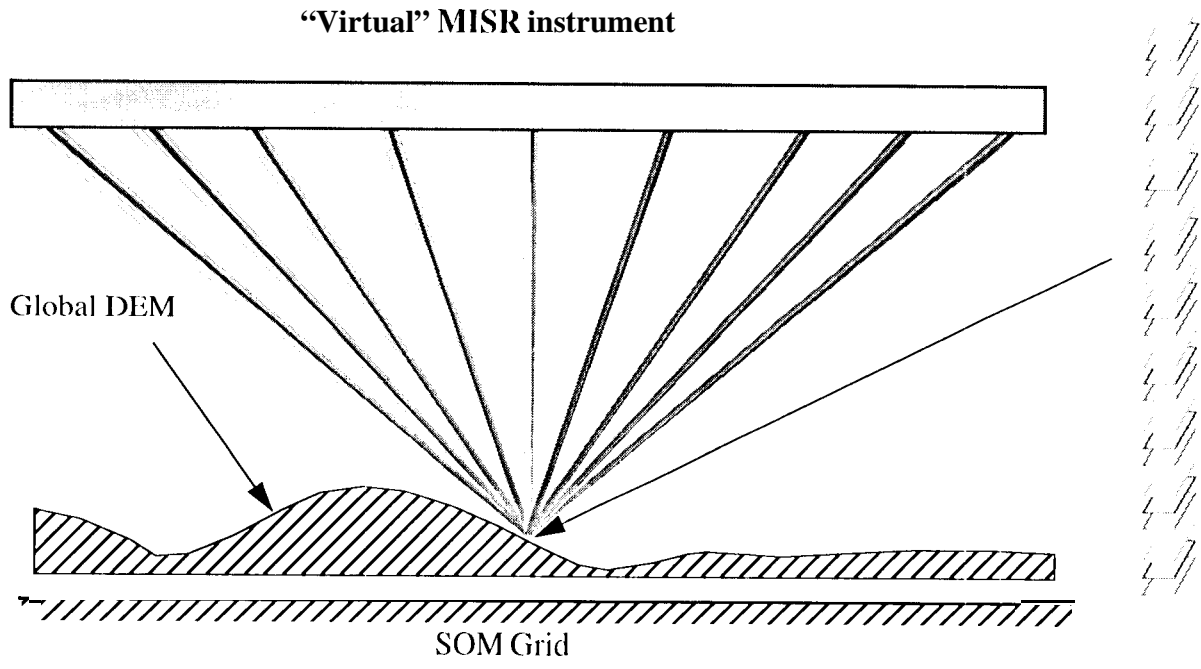
Terrain-projected red band data for A forward (Af) and C aft (Ca) cameras are superimposed to make this color composite. The Af camera image data are color coded red and the Ca camera image data are color coded blue and green to make a pseudo color image. Due to the terrain projection, parallax is removed and overlaid data appear like a single orthorectified image. The small regions of red pixels represent topographic obstructions to the viewing angle (see Section V.C). A significant portion of these pixels cannot be imaged by either Af or CA cameras.

MISR orbit - An_mar21_233_1426 (Day 1)

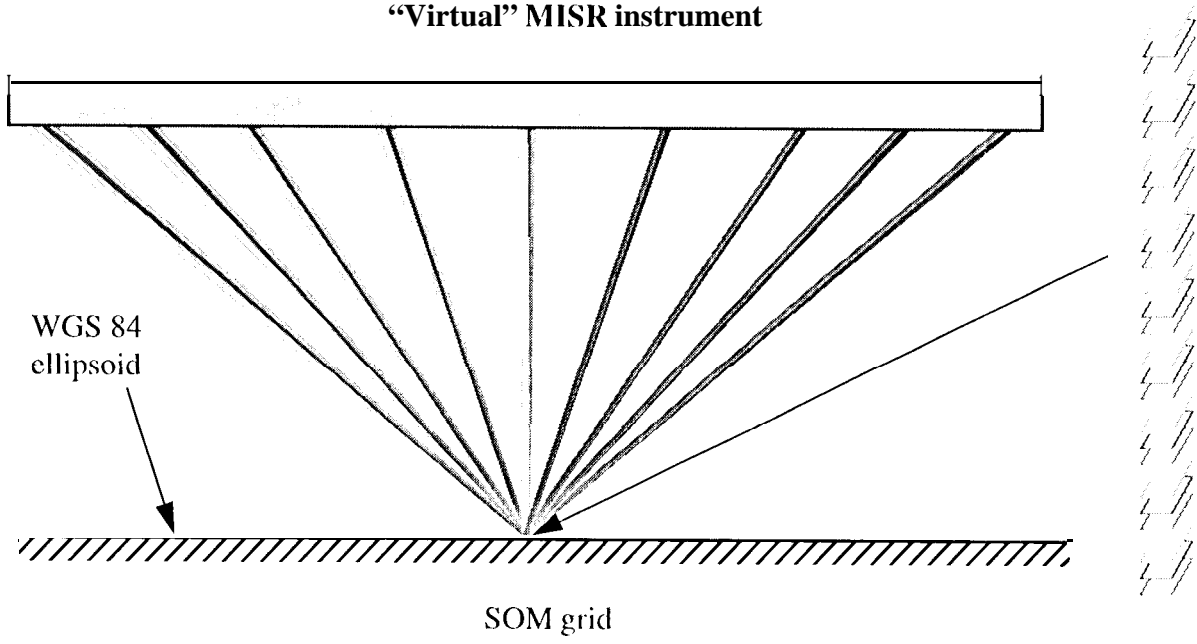


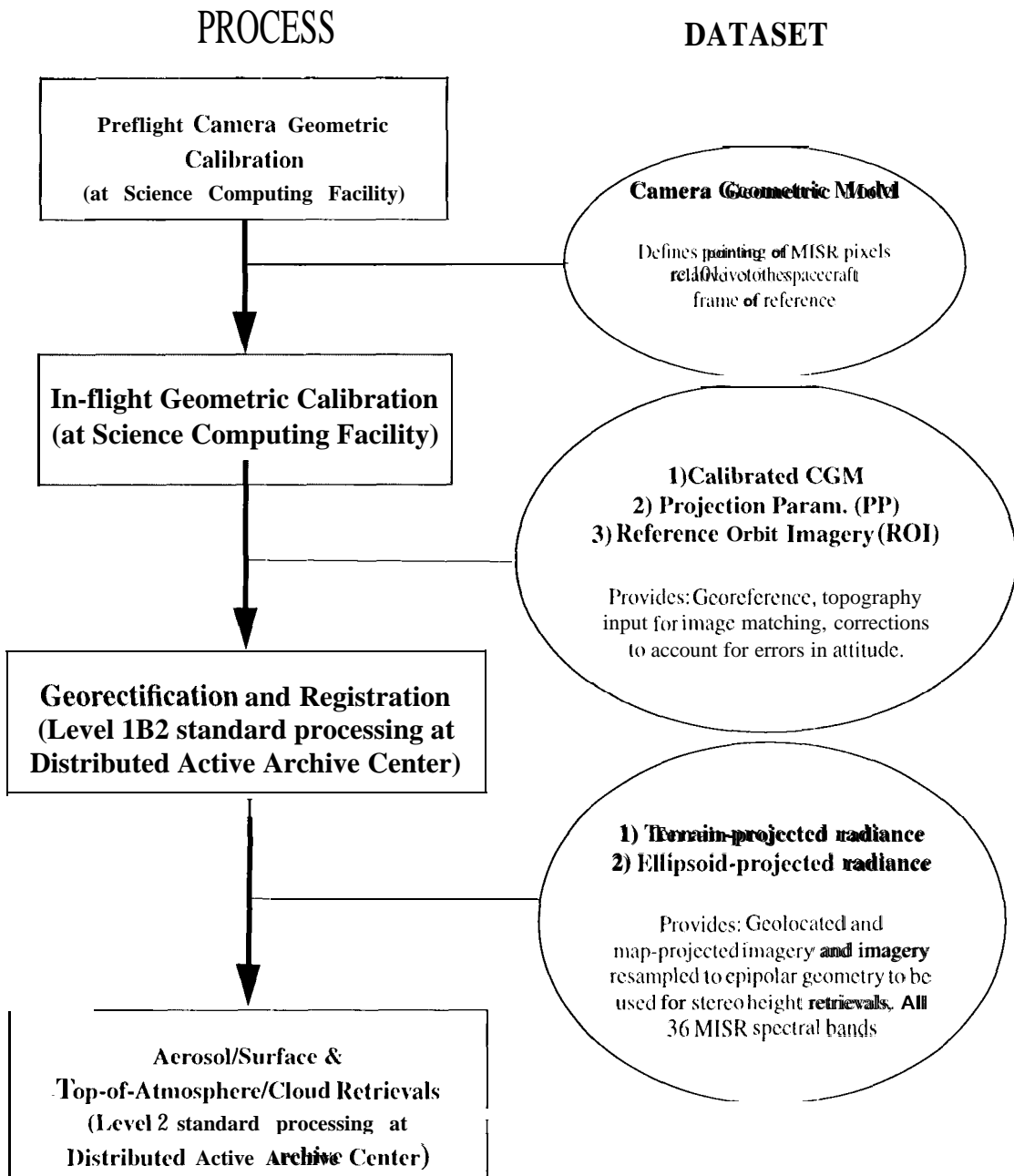
“Physical” MISR instrument

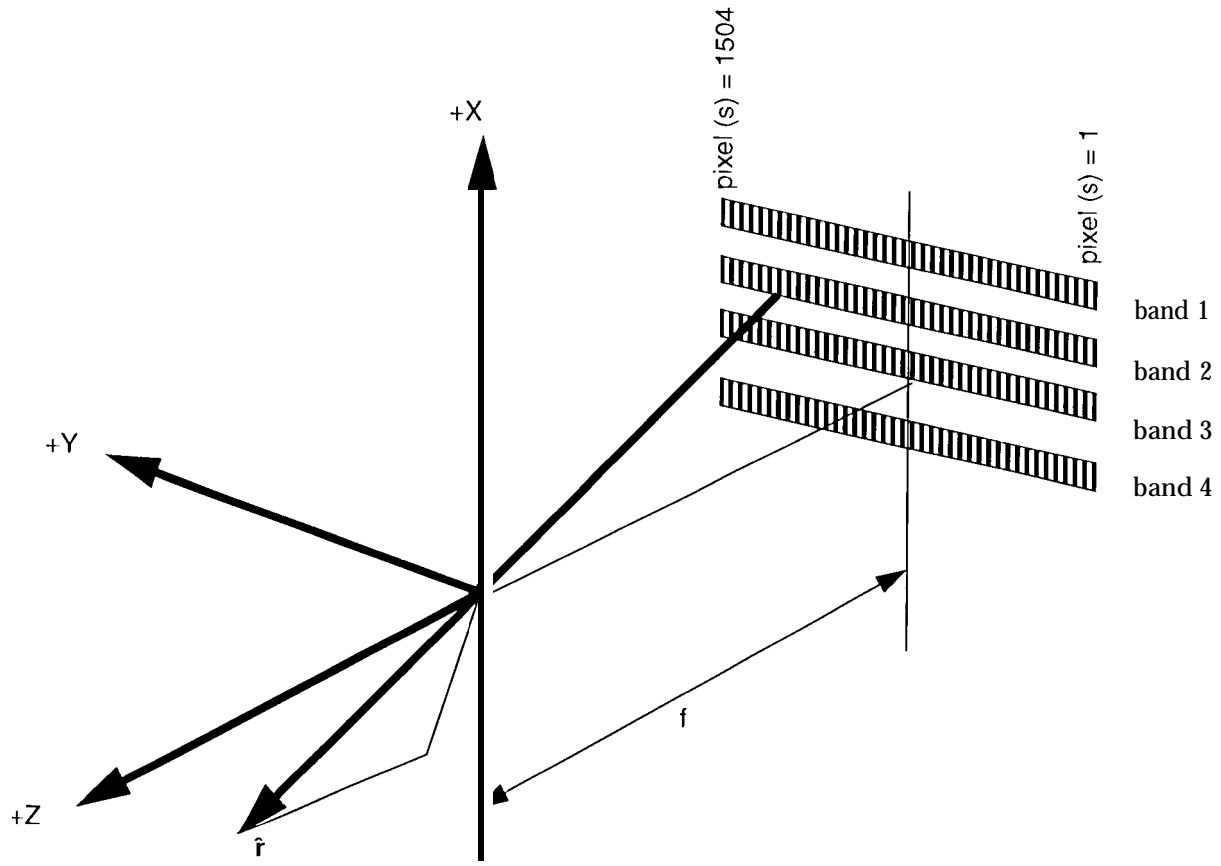




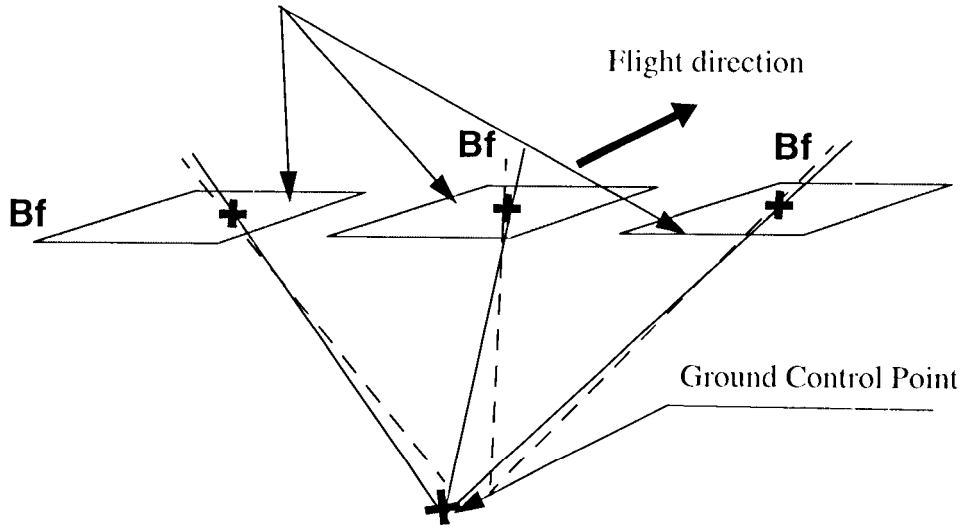
“Virtual” MISR instrument







Overlapping multiple
MISR imagery from
different orbit paths



———— True CGM
- - - - - Supplied CGM

